EPJ Web of Conferences **50**, 03004 (2013)
DOI: 10.1051/epjconf/20135003004

Calcite scale prediction at the near-well region: A radiotracer approach

E. Stamatakis[1,2,3], A. Stubos[1], T. Bjørnstad[2] and J. Muller[2]

[1] *National Centre for Scientific Research Demokritos, 15310 Agia Paraskevi, Attica, Greece*
[2] *Institute for Energy Technology, PO Box 40, 2027 Kjeller, Norway*
[3] *Centre for Renewable Energy Sources & Saving, 19009 Pikermi, Attica, Greece*

Abstract. Effective prediction of calcite scaling requires a reliable thermodynamic model for the prediction of the scaling tendency, a kinetic model for the prediction of scaling rate and a transport model to simulate flow in a porous medium. The accurate prediction of the scale deposition can warn the engineers to "treat" the formation around the wellbore in time. In addition, the prediction of the distribution of the scale deposition can direct the engineers to ensure the placement of the inhibitors into the formation zones where the deposition is expected, thus maximizing the probability of successful prevention of formation damage and minimizing at the same time the amount of the required inhibitors. In this contribution, we present a geochemical computational model that combines existing thermodynamic and kinetic models for $CaCO_3$ precipitation, with treatments of flow and diffusion in electrolyte systems, in an one-dimensional porous medium. The geochemical model has the ability to predict the distribution of scale deposition along and around the production wells, as well as the distribution of formation damage (pore blocking, permeability reduction) around the wells.

1. INTRODUCTION

The production, utilization and/or re-injection of brine found in petroleum reservoirs are often hampered by serious and very unique scale problems. Some of these scale problems are so severe that entire field operations are endangered. Effective scale management requires on-line monitoring of scaling tendencies as well as detection and identification of scale deposits.

Laboratory determinations of real-time scale deposition were recently reported using a radiotracer technique [1], an attenuated total reflection sensor [2], a rotating disk electrode technique [3], tapered optical fibers [4], a piezoelectric sensor [5] and an ultrasonic technique [6]. In addition, various nuclear attenuation techniques for the *in-situ* detection of mineral scale in actual production systems have been also reported recently. In particular, a handled device was developed to detect the presence of scale in surface piping by measuring the nuclear attenuation across the pipe diameter and two field cases were presented in which a dual-energy-venturi multiphase flow meter was used to detect and characterize scale according to the attenuation of the nuclear spectrum [7]. A year later, Poyet and co-researchers presented a gamma-ray attenuation method, based on continuous triple-energy gamma-ray attenuation measurements, for the detection of scale deposition in real-time in oilfield production tubulars [8].

The objective of the present work has been to demonstrate the use and applicability of the radiotracer technique for predicting calcite scale formation in oilfield applications. In that respect, a geochemical model, based on scale reaction calculations attempting to simulate/interpret dynamic tube-scale radiotracer experiments has been developed. The innovative feature of this model is the combination of thermodynamics, kinetics and hydrodynamics for the prediction of scale deposition along and around the production wells. Currently available models of $CaCO_3$ scale formation during flow in porous media, provide simply a scaling tendency. To assess a scale problem and manage deposition, it is important to know when, where and how much $CaCO_3$ will be deposited during oil production.

2. THE RADIOTRACER TECHNIQUE

The basis of this method is to label the calcium-containing liquid with the gamma emitter ^{47}Ca (in the chemical form of Ca^{2+}). The radioactive ^{47}Ca behaves chemically identical to non-radioactive calcium. When calcium carbonate precipitates, ^{47}Ca will be a messenger for where the precipitation takes place and to what degree (amount of precipitate). The gamma radiation from ^{47}Ca will penetrate the tube and be detected by external detectors. In this way, the radiotracer technique is an on-line non-intrusive and continuous experimental technique.

2.1. The experimental setup

The experimental setup is illustrated in Figure 1.

Twin HPLC pumps drive the two solutions (Brine 1 containing HCO_3^- & Brine 2 containing Ca^{2+}). The solutions are pumped through two pre-heating tubes that raise the solution temperature to the desired test temperature prior to arriving at the mixing point. The temperature is maintained constant by circulating heated Monoethylene Glycol (MEG; boiling point 198 °C) along the sand packed column, while the pressure is maintained constant using a back-pressure regulator at the outlet.

The combined supersaturated solution passes through the sand packed column and scale crystals nucleate and grow in the pore space. The sand packed columns consisted of 60 cm long stainless steel tubings with 1 cm ID, filled with quartz sand and are initially saturated with Brine 2 (containing $^{47}Ca^{2+}$).

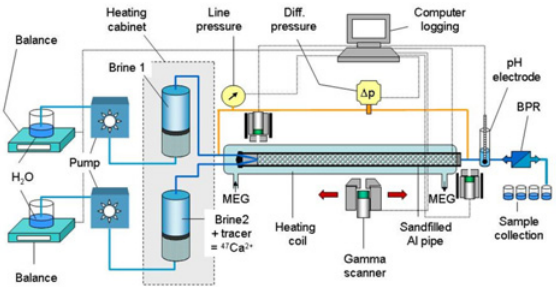

Figure 1. Experimental set-up illustration for the radiotracer technique.

The formation of scale is monitored by measuring the pressure drop (Δp) along the sand packed column, the change in pH after mixing the two solutions and the activity of ^{47}Ca in the deposit at the inlet. Three NaI(Tl) γ-detectors are used for the on-line measurements of ^{47}Ca activity. The first one (detector 1) is set at a fixed position at the inlet of the sand packed column dedicated to measure accurately the induction time, the second one (detector 2) is also set at a fixed position at the effluent dedicated to measure changes in Ca-concentration at the outlet, while the third one (γ-scanner) is used to monitor the growth of the calcite deposition along the sand packed columns. Samples are also collected periodically at the exit end of the sand packed column to be analyzed for ^{47}Ca.

The main gamma energy of ^{47}Ca is 1297 keV. However, by including also its Compton background and lower energies in the counting window, the sensitivity in the experiment may be increased. It is necessary to avoid contribution from ^{47}Sc, which is the daughter nuclide in the decay of ^{47}Ca. The energy window for the detectors will therefore be chosen from 350 keV and upwards to avoid the 159 keV γ-quanta from ^{47}Sc.

Samples are also collected periodically at the exit end of the sand packed column and the activity of ^{47}Ca (1297 keV) in solution determined in off-line high-resolution detector gamma-spectrometric measurements with a HpGe-detector coupled to a multichannel analyzer.

Solution temperature T_s, differential pressure Δp, pH, absolute system pressure p and $^{47}Ca^{2+}$ activity (count rate R) from the two on-line detectors are logged by computer during the experiment.

The *experimental* induction time of precipitation is defined as the time which elapses between the creation of supersaturation and the first observable change in some physical property of the precipitating (scaling) system, e.g. the appearance of crystals, change in solution conductivity, composition, pH, a change in pressure drop, etc. [9]. For the radiotracer method, in particular, the induction time is defined as the time which elapses between the first addition of $NaHCO_3$ solution into the sand packed column and the time when the count rate R significantly exceeds the statistical fluctuations of the initial (or background) count rate of $^{47}Ca^{2+}$ [10].

2.2. The radiotracer ^{47}Ca

^{47}Ca has a half-life of 4.54 days, and has to be produced by thermal neutron irradiation of Ca (^{46}Ca) in a nearby nuclear reactor. The following nuclear reaction takes place:

$$^{46}\mathrm{Ca(n,\gamma)}\,^{47}\mathrm{Ca}.$$

Natural calcium contains only 0.004% of the target nuclide ^{46}Ca. For low SR-values and reasonable uncertainty in the experiments, application of natural calcium as target material is insufficient. This argument will become clearer by studying the activation equation below where the number (N) of target nuclides is one of the parameters:

$$D = \sigma \cdot \phi \cdot \mathrm{N} \cdot (1 - e^{-\lambda t_i}) \cdot e^{-\lambda t_d}$$

where, σ = reaction cross section in cm^{-2}, φ = neutron flux (ncm^{-2}s^{-1}), N = number of target atoms, λ = decay constant ($= \ln 2/T_{1/2}$), t_i = irradiation time, t_d = decay time.

In natural Ca there is not sufficient number of ^{46}Ca-atoms to reach a disintegration rate, which is needed for saturation ratios in the order of 1.5 and slightly above. Calcium enriched in ^{46}Ca is needed, which can be found in the market. Here, isotopically enriched ^{46}Ca (4.1%) was used providing an 1000 times stronger target for irradiation. ^{47}Ca tracer was produced by irradiating the enriched calcium as $CaCO_3$ with thermal neutrons in IFE's nuclear reactor (JEEP II). The calculated activity (Bq) applied in the tests can be seen in the following table.

Ca-47 from enriched Ca-46 $CaCO_3$	
General input:	
Neutron flux (1/seconds*cm2):	9E+12
Cross section (barn):	0.7
Mass of target (g):	0.02854
Element mass fraction	0.4004
Mass of one target element nucleus (amu):	40.08
Isotopic fraction (%):	4.1
Half life (days):	4.54
Input: Radiation time (days):	3
Output: Radioactivity (MBq):	16.30

The irradiated $CaCO_3$ is then dissolved in HCl to produce ^{47}Ca tracer.

2.3. Calculation of the deposited calcite mass

$^{47}Ca^{2+}$ was used as tracer. ^{47}Ca emits gamma radiation, which can be measured online when the tracer is inside the sand packed column or in the collected samples. These measurements do not distinguish between $^{47}Ca^{2+}$ and $^{47}CaCO_3$. Thus, the total Ca concentration at the inlet of the sand packed column can easily be determined as follows:

$$[Ca]_t = [Ca]_o \frac{R_t}{R_o}$$

where $[Ca]_t$ is the total mol concentration of Ca (Ca^{2+} + $CaCO_3$) ions after time t, $[Ca]_0$ is the initial Ca concentration in the $^{47}CaCl_2$ solution, R_o is the initial

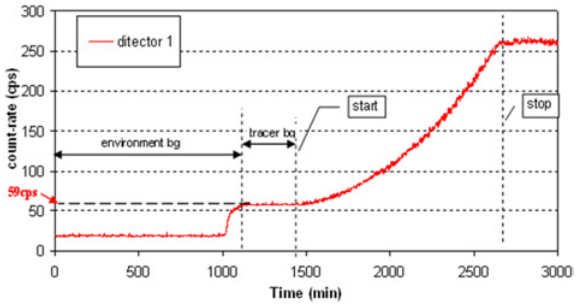

Figure 2. ^{47}Ca counting-rate at the inlet of the sand packed column.

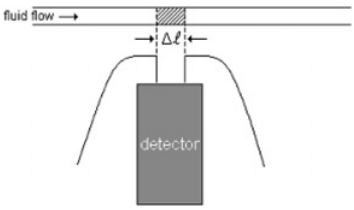

Figure 3. Gamma-scanner; $\Delta l = 0.2$ cm.

count-rate of $^{47}Ca^{2+}$ measured by the detector 1 at the inlet (tracer background; see Fig. 2) and R_t is the total count-rate of ^{47}Ca at the inlet after time t.

Then, assuming that Ca^{2+} conc. is constant at the inlet and equal to the feed stream conc., the $CaCO_3$ deposited mass at the inlet can be calculated as:

$$[CaCO_3]_t = [Ca]_o - [Ca]_t.$$

Moreover, a gamma scanner was used to measure the scale distribution along the sand packed column as described in paragraph 2.1. The gamma scanner consists of a collimated NaI(Tl) detector that can move along the sand packed column. The collimator is made of lead that ensures that the detector can only detect gamma radiation from a small slice of the sand packed column defined by the collimator opening (Fig. 3). Thus, by moving the detector and collimator along the sand packed column, the ^{47}Ca distribution can be measured.

To find the scale distribution along the sand packed column, the $^{47}Ca^{2+}$ cations must be removed from the sand packed column prior to the gamma scan, or their contribution must be subtracted from the total count-rate. At this point it has to be mentioned that the contribution of the scale on the reduction of the pore volume of the sand packed columns is negligible due to the small initial concentrations of the reactants. It has been confirmed both by calculations and measurements that no change in sand packed columns' porosity occurs.

The final deposited profile of $CaCO_3$ along the sand packed column can be calculated as:

$$\rho(x_j) = [Ca]_t \times \frac{R(x_j)}{d\sum_i R(x_i)}$$

where, ρ(xj) is mass deposited per unit length at position xj of the sand packed column, $[Ca]_t$ is the total mol concentration of Ca, d is the distance between the positions of two measurements and R(xj) is the count-rate of ^{47}Ca at position xj of the sand packed column.

3. DESCRIPTION OF THE MODEL

The main objective was to develop a formulation that can describe the carbonate system during flow in porous media. A one-dimensional (1D) transport model of multiple chemical species with simultaneous reversible and kinetically controlled reactions has been implemented in a lab-scale simulator. The conservation equations have been discretized using a finite volume approximation. The code has been successfully tested on the carbonate system [11], and some results relevant to the experimental work are presented below.

3.1. The chemical system

Calcite precipitation can be represented by a reversible overall reaction:

$$Ca^{2+} + CO_3^{2-} \rightleftharpoons CaCO_3(s). \quad \text{(I)}$$

Further reactions are necessary to describe the aqueous carbonate system. We assume one flowing phase only, and account for the following chemical reactions in that aqueous phase:

$$Ca^{2+} + CO_3^{2-} \rightleftharpoons CaCO_3^0(aq) \quad \text{(II)}$$

$$CO_2(aq) + H_2O \rightleftharpoons H^+ + HCO_3^- \quad \text{(III)}$$

$$Ca^{2+} + HCO_3^- \rightleftharpoons CaHCO_3^+(aq) \quad \text{(IV)}$$

$$HCO_3^- \rightleftharpoons H^+ + CO_3^{2-} \quad \text{(V)}$$

$$H_2O \rightleftharpoons H^+ + OH^-. \quad \text{(VI)}$$

Reaction (I) is kinetically controlled whereas the homogeneous reactions (II) to (IV) are considered to be reversible. The aqueous phase is prepared by dissolving $CaCl_2$ and $NaHCO_3$, and, all together, there are 11 species in the system ($CaCO_{3(s)}$, Ca^{2+}, CO_3^{2-}, $CaCO_{3(aq)}^0$, $CO_{2(aq)}$, H^+, HCO_3^-, $CaHCO_3^+$, OH^-, Cl^-, Na^+). The system of equations for the reaction/convection process will then consist of five conservation equations without reaction rate terms and one conservation equation with the rate term of the calcite precipitation, reaction (I). Adding five equilibrium constraints for the reversible reactions (II) to (IV), we obtain a total of 11 equations, a number equal to the number of species. The equilibrium conditions are computed using the aqueous solution model $CaCO_3$-NaCl-H_2O that includes the $CaHCO_3^+$ and $CaCO_3^0$(aq) ion pairs as suggested by Plummer & Busenberg [12]; the equilibrium constants for reactions [2] to [5] are taken from Plummer & Busenberg (1982), while for reaction [6] from Nordstrom et al. [13] (1990), both cited in Stumm & Morgan [14] (1996).

3.2. Conservation equations for reacting species

Without making any assumption about the nature of the chemical reactions, the conservation equation for each species "i" in single-phase flow is

$$\frac{\partial C_i}{\partial t} + div\mathrm{j}_i = \sum_k v_{ik} r_k \qquad (1)$$

where, C_i is the concentration of species i, r_k is the rate of reaction k, $div\mathbf{j}_i$ denotes the flux of species i and v denotes the stoichiometric coefficients. Such coefficients are, by convention, negative for the reactants and positive for the reaction products. Inclusion of solid components does not violate Equation (1) as long as the concentration of a solid component is interpreted as amount of substance per bulk volume unit. The flux of a solid component is zero, but the flux term is shown in the equations in order to preserve symmetry. Thus, with the reactions shown in equations (I) to (IV), and the aqueous solution made of dissolved $CaCl_2$ and $NaHCO_3$, the linear system of conservation equations corresponding to equation 1 can be written as:

$$\begin{bmatrix} \frac{\partial}{\partial t}C_{CO_2(aq)} + div\mathrm{j}_{CO_2(aq)} \\ \frac{\partial}{\partial t}C_{CO_3^{2-}} + div\mathrm{j}_{CO_3^{2-}} \\ \frac{\partial}{\partial t}C_{Ca^{2+}} + div\mathrm{j}_{Ca^{2+}} \\ \frac{\partial}{\partial t}C_{CaCO_3(o)} + div\mathrm{j}_{CaCO_3(o)} \\ \frac{\partial}{\partial t}C_{CaCO_3(s)} + div\mathrm{j}_{CaCO_3(s)} \\ \frac{\partial}{\partial t}C_{CaHCO_3^+} + div\mathrm{j}_{CaHCO_3^+} \\ \frac{\partial}{\partial t}C_{Cl^-} + div\mathrm{j}_{Cl^-} \\ \frac{\partial}{\partial t}C_{H^+} + div\mathrm{j}_{H^+} \\ \frac{\partial}{\partial t}C_{HCO_3^-} + div\mathrm{j}_{HCO_3^-} \\ \frac{\partial}{\partial t}C_{Na^+} + div\mathrm{j}_{Na^+} \\ \frac{\partial}{\partial t}C_{OH^-} + div\mathrm{j}_{OH^-} \end{bmatrix} = \begin{bmatrix} 0 & 0 & -1 & 0 & 0 & 0 \\ -1 & -1 & 0 & 0 & 0 & 1 \\ -1 & -1 & 0 & -1 & 0 & 0 \\ 0 & 1 & 0 & 0 & 0 & 0 \\ 1 & 0 & 0 & 0 & 0 & 0 \\ 0 & 0 & 0 & 1 & 0 & 0 \\ 0 & 0 & 0 & 0 & 0 & 0 \\ 0 & 0 & 1 & 0 & 1 & 1 \\ 0 & 0 & 1 & -1 & 0 & -1 \\ 0 & 0 & 0 & 0 & 0 & 0 \\ 0 & 0 & 0 & 0 & 1 & 0 \end{bmatrix} \begin{bmatrix} r_1^{irr} \\ r_2^{rev} \\ r_3^{rev} \\ r_4^{rev} \\ r_5^{rev} \\ r_6^{rev} \end{bmatrix}$$

In the system above, the rate terms are given a subscript corresponding to the reaction number [1] to [6]. In addition, the rate terms are given a superscript indicating whether the reaction is reversible (rev) or irreversible (irr).

After the various manipulations of the linear system of equations, aiming at the elimination of the reaction rates of the reversible reactions, the trivial conservation equation 1 for the n^{ion} chemical species is transformed into a system of equations consisted of:

$$\begin{Bmatrix} n^{rev} \text{ equilibrium constraints} & \sum_{\mathrm{i}} v_{ik}\mu_\iota = 0 \\ n^{ion} - n^{rev} - n^{irr} \text{ conservation equations} & \sum_{\mathrm{k}} \mathrm{A_{ik}}(\frac{\partial C_k}{\partial t} + div\mathrm{j}_k) = 0 \\ n^{irr} \text{ conservation equations with rate terms} & \sum_{\mathrm{k}} \mathrm{B_{ik}}(\frac{\partial C_k}{\partial t} + div\mathrm{j}_k) = r_i \end{Bmatrix}$$

where matrices **A**, **B** holds for $\mathbf{R} = \begin{bmatrix} \mathbf{A} \\ \mathbf{B} \end{bmatrix}$, $\mathbf{R} \cdot \mathbf{M} = \mathbf{0}$, and **M** the stoichiometric matrix of the reversible reactions, which is obtained after separating the right-hand-side of equation 1 into irreversible and reversible reactions

$$\left(\frac{\partial}{\partial t}\mathbf{C} + div\,\mathbf{J} = \mathbf{N}r^{irr} + \mathbf{M}r^{rev}\right).$$

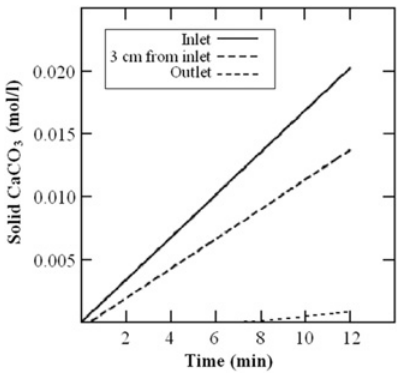

Figure 4. Model calculated calcite deposition growth at three positions in the column. The reaction rate term is shown in Equation (2).

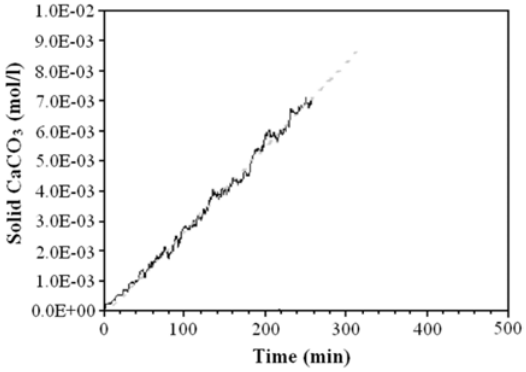

Figure 5. Real calcite deposition growth at the inlet of the sand packed column measured with the radiotracer technique for a specific run. It is clear the linear shape of the growth. The induction time has been eliminated.

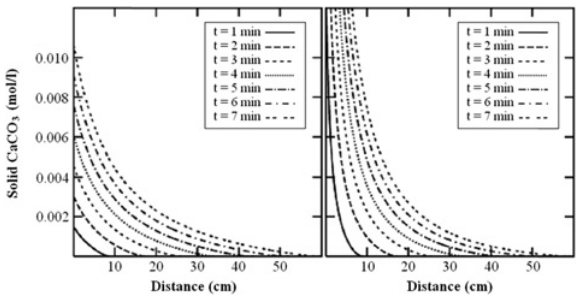

Figure 6. Calcite deposition for two different values of k_p^o. Left: $k_p^o = 161\ 149\,\mathrm{mol\,L^{-1}\,min^{-1}}$. Right: $k_p^o = 1\ 611\ 490\,\mathrm{mol\,L^{-1}\,min^{-1}}$.

3.3. Simulation of laboratory experiments and parameter estimation

In a previous work, certain rate equations from the literature have been tested against the experimental data [11]. Simulations of these data revealed that a linear rate equation with respect to supersaturation like the one proposed by Reddy & Nancollas [15], despite its simplicity, predicts satisfactorily $CaCO_3$ precipitation in the near well region.

$$\frac{d[CaCO_3]}{dt} = R_L = k_p^o(SR - 1) \qquad (2)$$

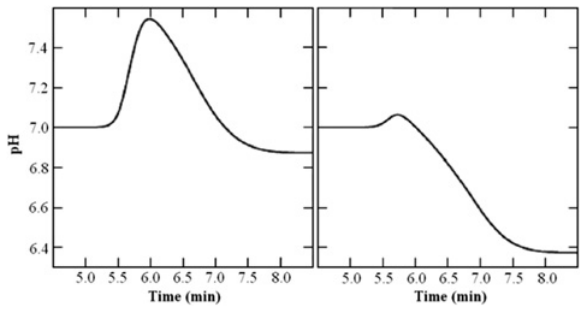

Figure 7. pH at the column outlet for two different values of k_p^o. Left: $k_p^o = 161\ 149\,\mathrm{mol\,L^{-1}\,min^{-1}}$. Right: $k_p^o = 1\ 611\ 490\,\mathrm{mol\,L^{-1}\,min^{-1}}$.

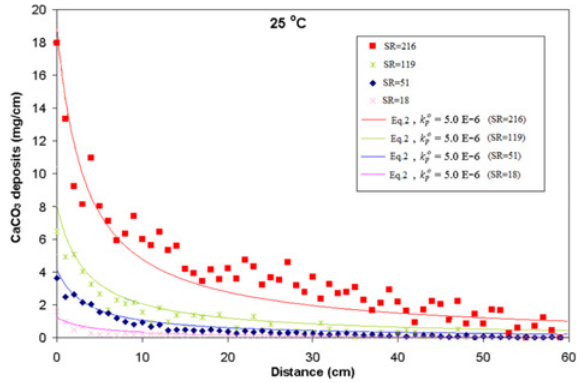

Figure 8. Deposited profiles of $CaCO_3$ at different saturation ratios at 25°C (q = 0.2 ml min^{-1}) using Equation (2).

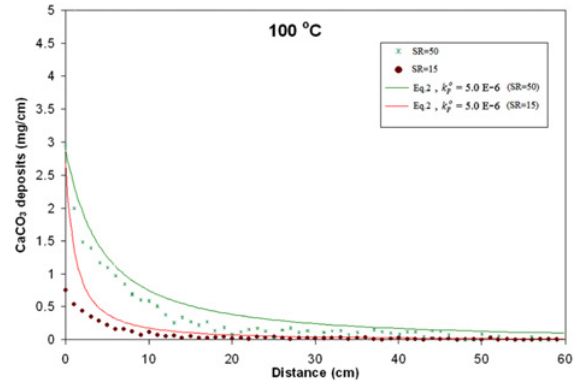

Figure 9. Deposited profiles of $CaCO_3$ at different saturation ratios at 100 °C (q = 0.2 ml min^{-1}) using Equation (2).

The calcite deposition rate will be constant at steady state conditions and, as a consequence, the calcite deposition is for all practical purposes linear in time. This effect is clearly seen in Figure 4. The linear shape of the calcite growth curve agrees with the experimental data (see Fig. 5). In order to perform a proper history matching, one must probably establish a reaction rate model that incorporates effects like primary and secondary precipitation. Those effects are ignored here.

The calcite deposition during flooding and the pH at the column outlet are measured during the experiments. These parameters, calculated using two different values for $\boldsymbol{k}_p^o$, are shown in Figures 6 and 7. The rate equations considered have different functional form, and as a consequence, the parameters in the two rates are of different order of magnitude.

For Reddy's reaction rate model (Eq. (2)), the curves in both Figures 8 and 9 are based on a value of the input parameter $k_p^o = 5.0 \times 10^{-6}\,\mathrm{mol\,L^{-1}\,min^{-1}}$ and being compared with the measured precipitation data (see paragraph 2.3 for details) at 25 and 100 °C, respectively.

4. CONCLUSIONS

A geochemical model, which simulates $CaCO_3$ scale formation during flow in porous media, has been developed. The model has the ability to predict the distribution of the scale precipitation in a 1D porous medium and the consequent pore blocking and not just the scaling tendency as all currently existing models do. The development of the geochemical model was based on scale reaction calculations attempting to simulate/interpret dynamic tube-scale laboratory experiments. The laboratory data have been acquired from a series of sand packed column blocking experiments using for the first time a radiotracer technique. Simulations of these data revealed that a rate equation like the one proposed by Reddy (Eq. (2)), despite its simplicity, predicts satisfactorily $CaCO_3$ precipitation in the near well region, by tuning the rate parameter k_p^o. In particular, it was found that using the value $k_p^o = 5.0 \times 10^{-6}\,\mathrm{mol\,L^{-1}\,min^{-1}}$, Eq. (2) fits well the experimental data over a wide range of temperatures (25–100 °C) and saturation ratios (15–216) tested in this study.

The geochemical module developed presently aims at advancing the understanding and promoting the prevention of formation damage during production due to calcite precipitation. The tool may assist the petroleum industry in designing efficient squeeze treatment methods of scaling prevention and to optimize in a cost-effective way certain aspects of the production and environmental policies of oil operator companies; the knowledge of the actual position of the forthcoming scale deposition can lead to the design of techniques that place the inhibitors only at the specific positions, thus reducing the amount of the inhibitor required to be squeezed.

References

[1] E. Stamatakis, A. Haugan, Ø. Dugstad, J. Muller, C. Chatzichristos, T. Bjørnstad, I. Palyvos, Chemical Engineering Science **60/5**, 1363–1370 (2005a)
[2] J.K. Smith, M. Yuan, T.H. Lopez, M. Means, J.L. Przybylinski, paper **SPE 80372** presented at the 5th International Oilfield Scale Symposium, Aberdeen, UK (2003)
[3] A.P. Morizot, A. Neville, paper **SPE 60189** presented at the 2nd International Oilfield Scale Symposium, Aberdeen, UK (2000)
[4] P.N. Moar et al., Journal of Applied Physics, 3395 (1999)
[5] D.H. Emmons, G.C. Graham, S.P. Holt, M.M. Jordan, B. Lorcardel, paper **SPE 56776** presented

at the SPE Annual Technical Conference and Exhibition, Huston, Texas (1999)
[6] G.P.P. Gunarathne, R.W. Keatch, paper **SPE 30418** presented at the Offshore Europe Conference, Aberdeen UK (1995)
[7] B. Theuveny, G. Ségéral, P.O. Moksnes, paper OTC 13152 presented at the Offshore Technology Conference, Houston, Texas (2001)
[8] J-P. Poyet, G. Ségéral, E. Toskey, paper SPE 74659 presented at the 4th International Oilfield Scale Symposium, Aberdeen, UK (2002)
[9] O. Söhnel, J.W. Mullin, Journal of Crystal Growth **60**, 239–250 (1982)
[10] E. Stamatakis, A. Stubos, I. Palyvos, C. Chatzichristos, J. Muller, Journal of Colloid and Interface Science **286/1**, 7–13 (2005b)
[11] E. Stamatakis, A. Stubos, J. Muller, Journal of Geochemical Exploration **108**, 115–125 (2011)
[12] L.N. Plummer, E. Busenberg, Geochimica et Cosmochimica Acta **46**, 1011–1040 (1982)
[13] D.K. Nordstrom, L.N. Plummer, D. Langmuir, E. Busenberg, H.M., May, B.F. Jones, D.L. Parkhurst, 1990. p. 398–413. In: D.C. Melchior and R.L. Bassett (ed.) Chemical modeling of aqueous systems II. Am. Chem. Soc., Columbus, OH
[14] W. Stumm, J.J. Morgan, 1996. Aquatic Chemistry. In: John Wiley & Son Inc. (3rd Ed.)